

## Spin-polarized surface states on Br/Ge(111)-(1×1): Surface spin polarization without heavy elements

Yoshiyuki Ohtsubo,<sup>1,2,\*</sup> Shinichiro Hatta,<sup>1,2</sup> Nobuhiko Kawai,<sup>1</sup> Akinobu Mori,<sup>1</sup> Yasuo Takeichi,<sup>3</sup> Koichiro Yaji,<sup>2,3</sup> Hiroshi Okuyama,<sup>1</sup> and Tetsuya Aruga<sup>1,2,†</sup>

<sup>1</sup>*Department of Chemistry, Graduate School of Science, Kyoto University, Kyoto 606-8502, Japan*

<sup>2</sup>*JST CREST, Saitama 332-0012, Japan*

<sup>3</sup>*Institute for Solid State Physics, University of Tokyo, 5-1-5 Kashiwanoha, Kashiwa, Chiba 277-8581, Japan*

(Received 19 July 2012; revised manuscript received 2 October 2012; published 31 October 2012)

We have investigated the atomic and electronic structure of the Br/Ge(111)-(1×1) surface. A couple of surface bands were found near the bulk valence band maximum by angle-resolved photoelectron spectroscopy (ARPES). Spin-resolved ARPES (SARPES) experiments showed that these surface bands are spin polarized. The results of the first-principles calculation based on the atomic structure determined by low-energy electron diffraction are in good agreement with the ARPES and SARPES results. The present result clearly shows that the significant spin polarization of the surface electronic states due to the Rashba spin-orbit interaction can be obtained without heavy elements belonging to the fifth or higher rows of the periodic table.

DOI: [10.1103/PhysRevB.86.165325](https://doi.org/10.1103/PhysRevB.86.165325)

PACS number(s): 61.05.jh, 73.20.At, 71.70.Ej

### I. INTRODUCTION

Spin-polarized electronic states are gathering much attention because of the possible application to spin transport phenomena.<sup>1,2</sup> The space inversion asymmetry at surfaces lifts the spin degeneracy of surface states due to the spin-orbit interaction (SOI). Such spin polarization on surfaces has been extensively studied for the surface-states spin split due to the Rashba-type<sup>3</sup> and other SOI<sup>4</sup> on surfaces as well as for spin-polarized gapless surface states formed on topological insulators.<sup>5,6</sup> It is understood that the large Rashba spin splitting, as observed on Au(111)<sup>7-9</sup> and other surfaces,<sup>10-16</sup> is induced by the large SOI due to heavy elements.<sup>17</sup>

For instance, the spin splitting of the L-gap surface state on <sub>79</sub>Au(111) amounts to 110 meV at the Fermi level  $E_F$  and the Rashba parameter  $\alpha_R$  is determined to be 0.36 eV Å.<sup>7</sup> On the other hand, the spin splitting for the surface state with the same origin on <sub>47</sub>Ag(111) is calculated to be 1.9 meV, which is too small to be observed experimentally, and  $\alpha_R$  is only 0.012 eV Å.<sup>18</sup> For topological insulators, the SOI derived from heavy elements also plays an important role in opening a large spin-orbit gap which often causes the spin-polarized gapless states,<sup>6</sup> such as those observed on Bi<sub>x</sub>Sb<sub>1-x</sub><sup>19</sup> and Bi<sub>2</sub>Se<sub>3</sub>.<sup>20</sup> Thus the studies of the surface spin polarization have been performed on the materials containing heavy elements, mostly in the sixth row of the periodic table. If the spin polarization of surface states without heavy element is found, it would expand the range of the material search for the surface spin transport.<sup>16</sup>

Recently, we have found a peculiar spin-polarized surface state on the Bi/Ge(111)-(√3 × √3)R30° surface.<sup>21</sup> The first-principles calculation indicated that these states are localized in subsurface Ge layers and the SOI of surface Bi atoms does not contribute to these spin polarizations. To the best of our knowledge, this is the only case where the Rashba-type surface spin polarization without the contribution of heavy elements was observed experimentally. Since these spin-polarized states were derived from the subsurface Ge atoms, similar spin-polarized states are expected to be formed on Ge(111) covered with lighter elements.

In order to verify the above hypothesis, we have studied in this work the electronic structure of the Ge(111) surface covered with a monolayer of bromine. Note that even the clean Ge(111) may also have similar spin-polarized surface bands. However the dangling-bond surface states on the clean surface may interfere with the observation of subsurface states. Bromine has an atomic number of 35, which is close to that of Ge, 32. Moreover the LEED result shown below indicates that Br terminates the dangling bonds of Ge(111), giving rise to Br-Ge bonding and antibonding states far below and above the Fermi level. Thus the Br/Ge(111) surface is associated with SOI comparable with clean Ge(111), while the dangling-bond surface states fully saturated, providing a most adequate surface to study subsurface electronic states in detail. We present the electronic structure of the Br/Ge(111)-(1×1) surface<sup>22-24</sup> studied by using angle-resolved photoelectron spectroscopy (ARPES), spin-resolved ARPES (SARPES), and first-principles calculation based on the atomic structure determined by dynamical low-energy electron diffraction (LEED) analysis. The surface bands were observed near the bulk valence band maximum (VBM) around  $\bar{\Gamma}$ . They are spin polarized perpendicular to both the surface normal and the wave vector, and are localized in the Ge subsurface region. Our results show unambiguously that significant spin polarization of Ge subsurface states occurs due to Rashba SOI without any contribution of heavy elements.

### II. EXPERIMENTAL AND COMPUTATIONAL METHODS

Experiments were performed in two separate ultrahigh vacuum chambers, one for LEED and ARPES, and the other for SARPES. The Ge(111) samples were cut from an *n*-type single crystal wafer. The clean Ge(111) surface was prepared by repeated cycles of Ar ion sputtering and annealing up to ~900 K until a sharp  $c(2\times 8)$  LEED pattern was obtained. Molecular Br<sub>2</sub> was produced by an electrochemical AgBr + CdBr<sub>2</sub> cell.<sup>25</sup> The Ge(111) sample was kept at 540 K during the exposure to Br<sub>2</sub> as well as after the exposure, which

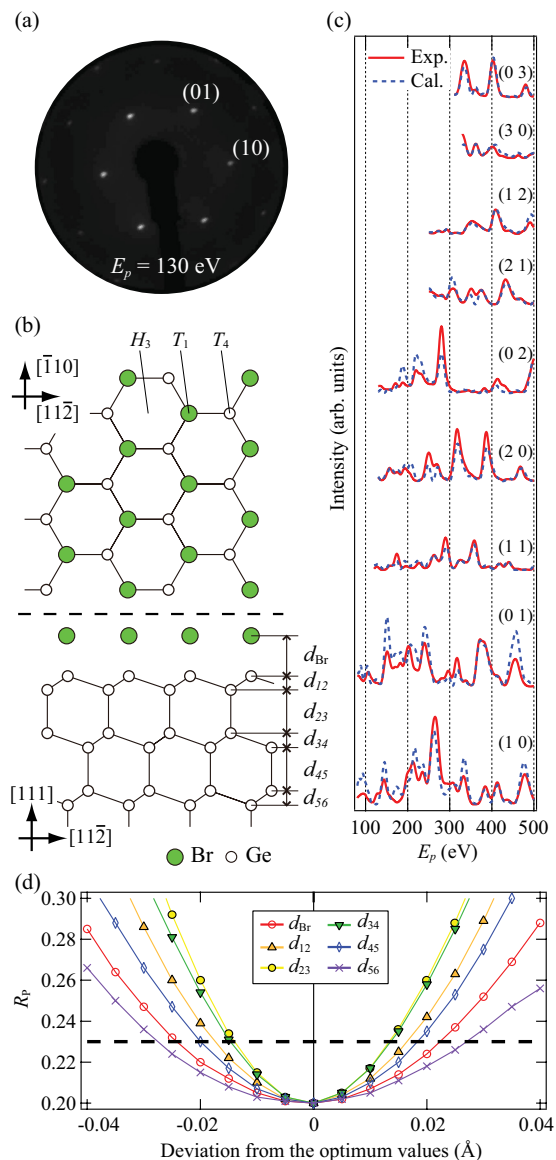


FIG. 1. (Color online) (a) LEED pattern of Br/Ge(111)-(1 $\times$ 1) at room temperature. (b) Top and side views of the optimized Br/Ge(111)-(1 $\times$ 1) surface. (c) Comparison of the experimental (full) and calculated (dashed)  $I$ - $V$  curves for the optimized  $T_1$  model. (d) The  $R_p$  values as a function of the deviation of the interlayer distances from the optimized values. Horizontal broken line indicates the  $R_p + RR$  value, which defines the errors.

yielded sharp and low-background (1 $\times$ 1) LEED patterns as shown in Fig. 1(a).

Normal-incidence LEED patterns at 80–500 eV were recorded at 100 K at an interval of 2 eV by a computer-controlled image acquisition system. The intensity versus voltage ( $I$ - $V$ ) curves were normalized by the primary beam current and averaged over the symmetrically equivalent beams according to the plane symmetry group  $p3m1$ . The obtained data set consisted of nine inequivalent beams, (1 0), (0 1), (1 1), (2 0), (0 2), (2 1), (1 2), (3 0), and (0 3), and had a total energy range of 1419 eV. The Barbieri–Van Hove symmetrized automated tensor LEED (SATLEED) package was used to simulate the  $I$ - $V$  curves.<sup>26</sup> Crystal potentials for Ge and

Br were described by phase shifts obtained by the Barbieri–Van Hove phase shift package. We used phase shifts up to  $l_{\max} = 10$  for the optimization of the atomic structure. The imaginary part of the inner potential was fixed at  $-5$  eV. The calculated and experimental  $I$ - $V$  curves were compared by means of the reliability factor defined by Pendry ( $R_p$ ).<sup>27</sup> The thermal effect was taken into account in the calculation by optimizing the Debye temperature for each atomic layer. The errors in the structural parameters were evaluated with the Pendry  $RR$  function.<sup>27</sup>

ARPES measurements were carried out with monochromatized He I and He II ( $h\nu = 21.2$  and 40.8 eV, respectively) radiations and a hemispherical electron analyzer at Kyoto. SARPES spectra were measured at BL-19A of KEK-PF with He I radiation and a hemispherical electron analyzer equipped with a high-yield spin polarimeter based on spin-dependent very low energy electron diffraction (VLEED).<sup>28</sup> All the measurements were done at room temperature. The energy resolutions for ARPES and SARPES were 10 and 70 meV, respectively.

All-electron full-potential density-functional theory (DFT) calculation was done by using the “augmented plane wave + local orbitals” method implemented in the WIEN2K code,<sup>29</sup> in order to obtain the energetically optimized surface atomic structure and its electronic structure. For structural optimization, the surface was modeled by symmetric slabs of 22 Ge layers with both sides covered with (1 $\times$ 1)-Br monolayers. All the atom positions were optimized until the root-mean-square force became smaller than 2 mRyd/a.u. For the calculation of the electronic structure with SOI taken into account, a symmetric slab of 52 layers was made by inserting 28 bulk Ge layers into the center of the optimized 22-layer slab.

### III. RESULTS AND DISCUSSION

#### A. Atomic structure

The Br adsorption on the Ge(111) surface induces the well-ordered (1 $\times$ 1) structure at the coverage of 1 ML.<sup>22–24</sup> Here, the coverage is defined as the fraction of the topmost-layer atomic density of the bulk-truncated Ge(111) surface. The atomic structure of Br/Ge(111)-(1 $\times$ 1) was previously studied with the x-ray standing wave (XSW) technique<sup>22</sup> and scanning tunneling microscopy (STM).<sup>24</sup> In these studies, it was concluded that the Br atoms are adsorbed on the  $T_1$  sites of the bulk-truncated Ge(111) surface. On the other hand, less information was obtained about the displacements of substrate Ge atoms.

In the dynamical LEED analysis, we examined three structure models with unity Bi coverage, in which Br atoms are located on the threefold symmetry sites,  $H_3$ ,  $T_1$ , and  $T_4$ , as shown in Fig. 1(b). We optimized the atomic positions of Br and Ge atoms in the first six layers for the three models. The displacements were done in the way according to the plane symmetry group  $p3m1$ . The calculated  $R_p$  values are listed in Table I. The  $T_1$  model yielded a notably small  $R_p$  value of 0.20. Since the variance of  $R_p$  was 0.03, the other models were ruled out. The Debye temperatures for Br, Ge1, and Ge2 atoms were optimized to be 180, 230, and 330 K, respectively (Ge atoms in the  $n$ th layer are denoted  $Ge_n$  below). Those for the deeper layers were fixed at the bulk value (374 K). The comparison between the experimental and simulated  $I$ - $V$  curves shows a good overall agreement as shown in Fig. 1(c).

TABLE I. The  $R_P$  values and total energies ( $E_{\text{tot}}$ ) for the examined models.

Model	$R_P$	$E_{\text{tot}}$ (eV)
$H_3$	0.52	0.79
$T_1$	0.20	0.00
$T_4$	0.56	1.24

Figure 1(d) shows the  $R_P$  values as a function of the deviation of interlayer distances from the optimized values. The broken line, which corresponds to  $R_P + RR = 0.23$ , defines the errors. The interlayer distances  $d_{12}$  and  $d_{23}$  are most accurately determined with the errors  $\sim 0.015$  Å. While the 6th layer is located at  $\sim 10$  Å from the surface, the  $d_{56}$  distance is determined with an accuracy of  $\sim 0.025$  Å, because the  $I$ - $V$  curves were measured up to 500 eV, which was high enough to probe the deeper layers.

In Table I, the total energies for the three models obtained from the first-principles calculation are also listed. In the structural optimization calculation, we used the PBE96 generalized gradient approximation (GGA).<sup>30</sup> The  $T_1$  model was the most stable among the three models. As listed in Table II, the interlayer distances determined by the dynamical LEED analysis and the first-principles calculation agree well.

The results indicate that Br atoms occupy the  $T_1$  site. The Br-Ge distance is 2.29 Å, which is almost the same as the interatomic distance in the  $\text{GeBr}_4$  molecule (2.27 Å). As shown in Table II, the interlayer distances on the optimized surface deviate significantly from the bulk value only in the first bilayer, while those in the deeper layers are almost equal to the bulk values. The decrease in the first bilayer indicates the partial rehybridization of the Ge1 valence orbitals from  $sp^3$  toward  $sp^2 + p_z$ ,<sup>31</sup> which would be due to the polar bonding of Ge1 with more electronegative Br. The work function was determined by ARPES to be 5.60 eV, which is 0.99 eV larger than that of the clean Ge(111)- $c(2 \times 8)$  surface. The large increase of the work function is in agreement with the adsorption of electronegative Br atoms on top of the surface Ge atoms.

## B. Electronic structure

Figure 2(a) shows schematically the bulk Ge band structure. The valence bands of Ge are composed of heavy-hole and light-hole bands, and a spin-orbit split-off band as shown by the solid curves. The light-hole and spin-orbit split-off bands hybridize with each other to give actual energy bands as shown

TABLE II. The interlayer distances in Å defined as shown in Fig. 1(b). The errors are in parentheses. Bulk values are shown for comparison.

Parameter	LEED (this work)	DFT (this work)	XSW (Ref. 21)	Bulk
$d_{\text{Br}}$	2.29 (0.02)	2.28	2.21 (0.03)	
$d_{12}$	0.76 (0.02)	0.77		0.82
$d_{23}$	2.47 (0.02)	2.44		2.45
$d_{34}$	0.81 (0.02)	0.82		0.82
$d_{45}$	2.47 (0.02)	2.44		2.45
$d_{56}$	0.82 (0.03)	0.81		0.82

by the dashed curves in Fig. 2(a). While the characters of the latter two bands are interconverted at larger  $k$ , these final bands are labeled as HH, LH, and SO for convenience.

Figures 2(b) and 2(c) show the band dispersion near  $\bar{\Gamma}$  along  $\bar{\Gamma}\bar{K}$  measured by ARPES with He I and He II. The photoelectron intensity is plotted in gray scale. The bulk VBM is determined to be 0.06 eV below  $E_F$  by fitting the calculated bulk Ge bands. The dashed lines in Figs. 2(b) and 2(c) indicate the upper edges of the bulk HH, LH, and SO bands calculated with the empirical tight-binding method with parameters adjusted to the experimental bulk band structure.<sup>32</sup> The feature denoted as  $S$  is observed at the same energy for He I and II, and appears to be inconsistent with the bulk LH or SO bands, suggesting that it is a surface resonance.

The triangles in Fig. 2(d) show the spin-resolved momentum distribution curves (MDCs) taken at a binding energy of 0.2 eV along  $\bar{\Gamma}\bar{K}$ . The VLEED spin polarimeter is set to be sensitive to the spin polarization perpendicular to  $\bar{\Gamma}\bar{K}$  and the surface normal (parallel/antiparallel to  $[11\bar{2}]$ ). The spin polarization along this direction is expected from the inversion asymmetry along the surface normal and observed for various surface states on the Rashba systems. The solid line in Fig. 2(d) shows a spin-integrated MDC taken with He I. The spin-resolved MDC exhibits two pairs of peaks with the spin polarization at  $\pm 0.02$  Å<sup>-1</sup> and  $\pm 0.15$  Å<sup>-1</sup>. Note that the majority spin component of each peak in the spin-resolved MDC is oriented to the opposite directions for positive and negative  $k_{\parallel}$ , which is consistent with the surface mirror symmetry. This, on the other hand, is inconsistent with spin polarization induced in the photoexcitation process,<sup>33,34</sup> implying that the observed spin polarization is due to the initial-state spin polarization due to the Rashba effect.<sup>8,9,35</sup> The spin-polarized features at  $\pm 0.02$  Å<sup>-1</sup> are observed also in spin-integrated MDC, which corresponds to the  $S$  band identified in Figs. 2(b) and 2(c). This supports the assignment of  $S$  to a surface band. The spin-resolved MDC also exhibits spin-polarized peaks at  $\pm 0.15$  Å<sup>-1</sup>, which is very close to the bulk band edge of HH. This implies that another spin-polarized surface band exists near HH, while it is not clearly observed in ARPES. This will be further examined below in terms of the first-principles calculation.

In our first-principles calculation, we adopted the modified Becke and Johnson (mBJ) potential together with the exchange-correlation potential constructed by using the local density approximation (LDA).<sup>36,37</sup> In this way, we obtained the correct band gap for the electronic structure of the bulk Ge crystal. The band gap for bulk Ge is obtained to be 0.75 eV by using this method; the experimental value is 0.744 eV at  $T = 0$  K.<sup>38</sup> It has been confirmed that semiconductor surface states can be obtained by means of this method with almost the same accuracy as the other widely used methods such as GGA.<sup>4</sup>

Figure 3 shows the calculated states along  $\bar{\Gamma}\bar{K}$ . The contrasts (colors, online) of the circles represent the spin polarization orientation of each state. The radii of the circles  $R_{k_{\parallel}, E}$  are defined by the function

$$R_{k_{\parallel}, E} \propto \left| \sum_{i=0}^6 (|\langle \phi^i, \uparrow | \Psi_{k_{\parallel}, E} \rangle|^2 - |\langle \phi^i, \downarrow | \Psi_{k_{\parallel}, E} \rangle|^2) \right|, \quad (1)$$

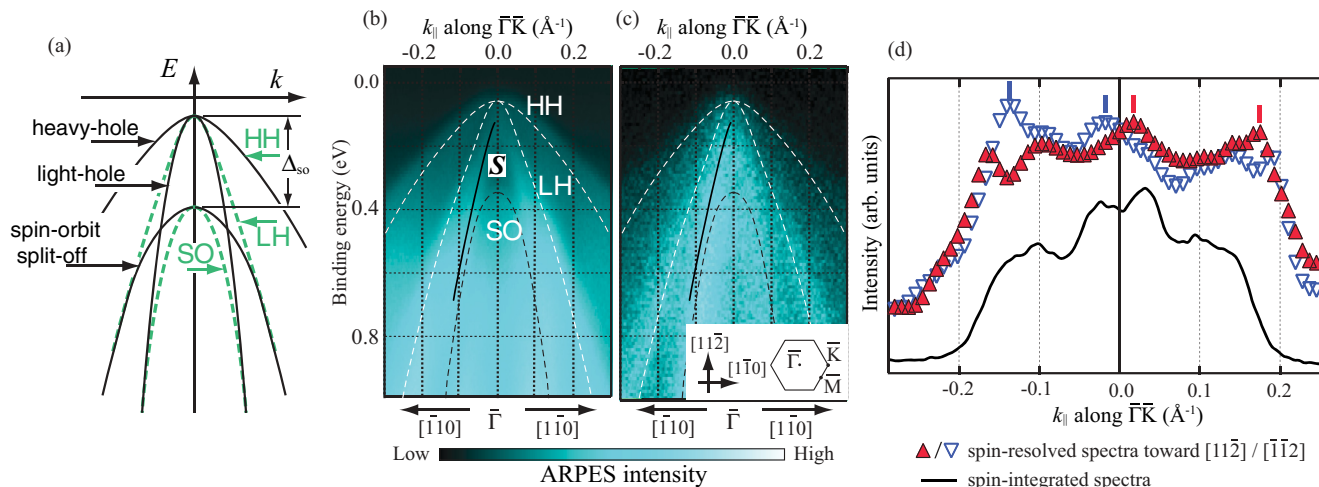


FIG. 2. (Color online) (a) Schematic of bulk Ge band structure (see text). At  $\Gamma$  the SO band is split by  $\Delta_{so} = 0.29$  eV from VBM. (b) ARPES image measured with He I. Dashed white lines indicate the bulk band edges. Solid line is a guide to the eyes. (c) Same as (b) but measured with He II. The inset shows the surface Brillouin zone. (d) Triangles indicate spin-resolved MDC measured at a binding energy of 0.2 eV. The effective Sherman function was 0.30. Solid line shows spin-integrated MDC deduced from the ARPES data shown in (b) at a binding energy of 0.2 eV.

where  $|\phi^i, \uparrow\rangle$  ( $|\phi^i, \downarrow\rangle$ ) represents the atomic orbital in the  $i$ th layer (the 0th layer corresponds to the Br adlayer) with spin polarization toward  $[11\bar{2}]$  ( $[\bar{1}\bar{1}2]$ ), and  $|\Psi_{k_{\parallel}, E}\rangle$  is the wave function of the calculated state at  $(k_{\parallel}, E)$ . Thus, the large circles in Fig. 3 represent the states which are spin polarized toward  $[11\bar{2}]$  or  $[\bar{1}\bar{1}2]$  and localized in the surface/subsurface

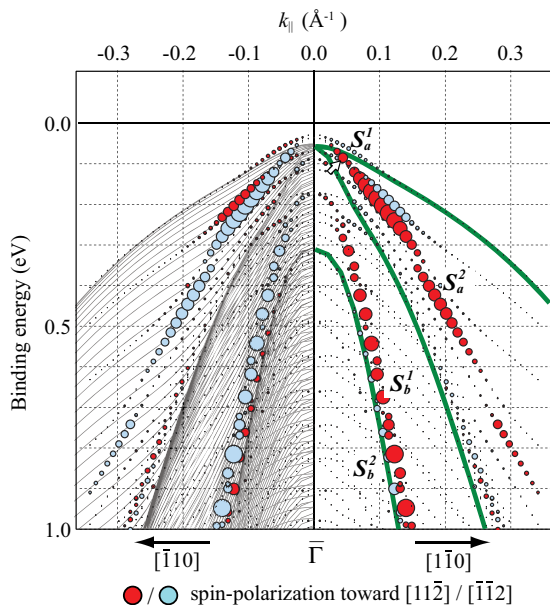


FIG. 3. (Color online) Calculated band structure along  $\Gamma\bar{K}$  for the slab with 50 Ge layers covered with Br monolayers on both side. The radii of the circles are defined by the function written in the text (1). The contrasts (colors, online) of the circles represent the spin polarization orientation of each state. On the left side, the projected bulk valence bands (thin lines) are shown. Solid lines on the right side represent the bulk bands dispersing across  $\Gamma$  in the bulk Brillouin zone.

layers. On the left side, the projected bulk bands onto the  $(111)$  surface are shown together (thin lines). Solid lines on the right side represent the upper edges of the bulk bands.

Electronic states localized in surface and subsurface layers form two bands,  $S_a$  and  $S_b$ , dispersing along the edges of the LH and SO bands, respectively.  $S_a$  is composed of two spin-polarized branches,  $S_a^1$  (upper one) and  $S_a^2$  (lower one), as denoted in Fig. 3. The  $S_a^1$  and  $S_a^2$  branches degenerate at  $\bar{\Gamma}$  at  $\sim 30$  meV above VBM, and are spin polarized toward  $[\bar{1}\bar{1}2]$  and  $[11\bar{2}]$ , respectively, for  $k_{\parallel}$  in the  $[1\bar{1}0]$  direction. The polarization direction is reversed for  $k_{\parallel}$  in the  $[\bar{1}10]$  direction. These features indicate that  $S_a^1$  and  $S_a^2$  are a Rashba spin-split pair. The  $S_b$  band also appears to be composed of upper ( $S_b^1$ ) and lower ( $S_b^2$ ) branches, which are spin polarized in a way similar to that of  $S_a^1$  and  $S_a^2$ . However, the spin-split pair structure is not very clear near the  $\bar{\Gamma}$  point. We suggest that this is due to the hybridization with bulk bands which have a large projected density of states near VBM.

Let us compare the spin-polarized electronic structures obtained by ARPES, SARPES, and the first-principles calculation. The surface band  $S$  observed by ARPES corresponds well to the calculated  $S_b$  band. The spin-polarized features at  $\pm 0.02$   $\text{\AA}^{-1}$  correspond to  $S_b^1$ . The calculated  $S_a^2$  branch explains well the spin-polarized signal observed at  $\pm 0.15$   $\text{\AA}^{-1}$  by SARPES. The contribution of  $S_a^1$  is not very clear in spin-polarized MDC, which may be due to the limited angular/energy resolution. Small humps at  $\pm(0.18-0.2)$   $\text{\AA}^{-1}$  in the spin-resolved MDC spectra may correspond to  $S_a^1$ .

Figure 4 shows the layer-resolved partial charge distribution for the state belonging to  $S_a^2$  (indicated by an arrow in Fig. 3). The envelope of the partial charge distribution has a maximum at around the first to fourth Ge bilayers, then gradually decays with the depth, and mostly diminishes at around the 20th layer. The states belonging to  $S_a^1$  and  $S_b^1$ , located near this state, have similar shapes of the envelopes. The spin polarization direction of each layer is uniform irrespective of the depth from the

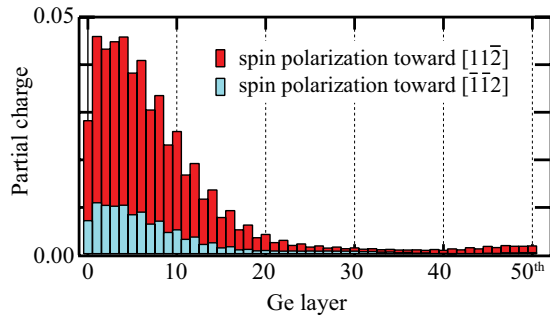


FIG. 4. (Color online) Layer- and spin-resolved partial charges of the states belonging to  $S_a^2$  at  $k_{\parallel} = 0.05 \text{ \AA}^{-1}$  (indicated by an arrow in Fig. 3). The zeroth and the 51st layers correspond to the Br adlayers.

surface. This is in marked contrast with the beating of the spin orientation with the distance from the surface which was reported for the bulk-continuum states spin polarized due to the reflection of the relativistic Bloch waves at the surface.<sup>39</sup> Note that since we used a symmetric slab with both sides terminated with Br, the computed band structure is composed of degenerate pairs of states localized near the top and bottom of the slab. The states at the top and bottom sides have mirror-symmetric depth profiles and are spin polarized in opposite directions. The states localized near the 0th layer was picked up and are shown in Figs. 3 and 4.

The calculation showed that the spin-polarized states belonging to  $S_a$  and  $S_b$  are derived dominantly from Ge  $4p_{xy}$  atomic orbitals in the subsurface layers. This character and the gradually decaying feature of the partial charge are very similar to those of the spin-polarized surface bands observed on Bi/Ge(111),<sup>21</sup> suggesting that they are intrinsic two-dimensional states formed on the Ge(111) surface. We believe that similar spin-polarized surface states would also be formed on Ge(111) surfaces covered with other adsorbates.

Actually, similar surface bands near bulk VBM have also been observed on Pb/Ge(111)- $\beta$ - $(\sqrt{3} \times \sqrt{3})R30^\circ$ .<sup>16,40</sup>

The spin-split branches of  $S_a$  degenerate at  $\Gamma$  and are spin split at finite  $k_{\parallel}$ , which is in good agreement with the Rashba spin splitting. The size of the splitting between  $S_a^1$  and  $S_a^2$  was calculated to be  $\sim 40 \text{ meV}$  at  $0.05 \text{ \AA}^{-1}$ , which yields the Rashba parameter  $\alpha_R = 0.4 \text{ eV \AA}$ . This is an order of magnitude smaller than those observed on surface bands derived from heavy elements. For instance, the Bi- $6p$ -derived surface state on Bi/Ge(111) exhibits a Rashba spin splitting with  $\alpha_R = 1.8 \text{ eV \AA}$ .<sup>14</sup> This difference in magnitude is consistent with that of atomic spin-orbit splitting of valence  $p$  orbitals: Bi (1.95 eV) and Ge (190 meV).<sup>41</sup> The result indicates that the maximum size of the Rashba spin splitting on surface bands is correlated with the atomic SOI and hence the significant spin splitting on the order of 100 meV can be realized only with the elements in the fourth row of the periodic table.

#### IV. CONCLUSION

The spin polarization of surface bands was observed on Br/Ge(111)- $(1 \times 1)$  by using SARPES. The first-principles calculation revealed that they are due to Rashba SOI in subsurface Ge layers. The result supports the previous conclusion that the spin polarization of Ge subsurface states on Bi/Ge(111) was also induced by the Ge SOI; it is not due to the scattering of bulk states by the Bi adlayer. The size of the spin splitting on surface bands is correlated with the size of atomic SOI, which clearly indicates a possibility of Ge-based spintronic applications.

#### ACKNOWLEDGMENT

The spin-resolved ARPES experiment has been performed under the approval of the Photon Factory Advisory Committee (PF-PAC No. 2009G195).

\*yoshiyuki.ohtsubo@synchrotron-soleil.fr

†aruga@kuchem.kyoto-u.ac.jp

<sup>1</sup>S. A. Wolf, D. D. Awschalom, R. A. Buhrman, J. M. Daughton, S. von Molnar, M. L. Roukes, A. Y. Chtchelkanova, and D. M. Treger, *Science* **294**, 1488 (2001).

<sup>2</sup>D. D. Awschalom and M. E. Flatté, *Nat. Phys.* **3**, 153 (2007).

<sup>3</sup>E. I. Rashba, *Sov. Phys. Solid State* **2**, 1109 (1960); Y. A. Bychkov and E. I. Rashba, *JETP Lett.* **39**, 78 (1984).

<sup>4</sup>Y. Ohtsubo, S. Hatta, H. Okuyama, and T. Aruga, *J. Phys.: Condens. Matter* **24**, 092001 (2012).

<sup>5</sup>C. L. Kane and E. J. Mele, *Phys. Rev. Lett.* **95**, 146802 (2005).

<sup>6</sup>L. Fu and C. L. Kane, *Phys. Rev. B* **76**, 045302 (2007).

<sup>7</sup>S. LaShell, B. A. McDougall, and E. Jensen, *Phys. Rev. Lett.* **77**, 3419 (1996).

<sup>8</sup>M. Hoesch, M. Muntwiler, V. N. Petrov, M. Hengsberger, L. Patthey, M. Shi, M. Falub, T. Greber, and J. Osterwalder, *Phys. Rev. B* **69**, 241401 (2004).

<sup>9</sup>J. Henk, M. Hoesch, J. Osterwalder, A. Ernst, and P. Bruno, *J. Phys.: Condens. Matter* **16**, 7581 (2004).

<sup>10</sup>Yu. M. Koroteev, G. Bihlmayer, J. E. Gayone, E. V. Chulkov, S. Blügel, P. M. Echenique, and Ph. Hofmann, *Phys. Rev. Lett.* **93**, 046403 (2004).

<sup>11</sup>T. Nakagawa, O. Ohgami, Y. Saito, H. Okuyama, M. Nishijima, and T. Aruga, *Phys. Rev. B* **75**, 155409 (2007).

<sup>12</sup>C. R. Ast, J. Henk, A. Ernst, L. Moreschini, M. C. Falub, D. Pacilé, P. Bruno, K. Kern, and M. Grioni, *Phys. Rev. Lett.* **98**, 186807 (2007).

<sup>13</sup>I. Gierz, T. Suzuki, E. Frantzeskakis, S. Pons, S. Ostanin, A. Ernst, J. Henk, M. Grioni, K. Kern, and C. R. Ast, *Phys. Rev. Lett.* **103**, 046803 (2009).

<sup>14</sup>S. Hatta, T. Aruga, Y. Ohtsubo, and H. Okuyama, *Phys. Rev. B* **80**, 113309 (2009).

<sup>15</sup>K. Sakamoto, H. Kakuta, K. Sugawara, K. Miyamoto, A. Kimura, T. Kuzumaki, N. Ueno, E. Anese, J. Fujii, A. Kodama, T. Shishidou, H. Namatame, M. Taniguchi, T. Sato, T. Takahashi, and T. Oguchi, *Phys. Rev. Lett.* **103**, 156801 (2009).

<sup>16</sup>K. Yaji, Y. Ohtsubo, S. Hatta, H. Okuyama, K. Miyamoto, T. Okuda, A. Kimura, H. Namatame, M. Taniguchi, and T. Aruga, *Nat. Commun.* **1**, 17 (2010).

- <sup>17</sup>L. Petersen and P. Hedegard, *Surf. Sci.* **459**, 49 (2000).
- <sup>18</sup>G. Nicolay, F. Reinert, S. Hüfner, and P. Blaha, *Phys. Rev. B* **65**, 033407 (2001).
- <sup>19</sup>D. Hsieh, D. Qian, L. Wray, Y. Xia, Y. S. Hor, R. J. Cava, and M. Z. Hasan, *Nature (London)* **452**, 970 (2008).
- <sup>20</sup>Y. Xia, D. Qian, D. Hsieh, L. Wray, A. Pal, H. Lin, A. Bansil, D. Grauer, Y. S. Hor, R. J. Cava, and M. Z. Hasan, *Nat. Phys.* **5**, 398 (2009).
- <sup>21</sup>Y. Ohtsubo, S. Hatta, K. Yaji, H. Okuyama, K. Miyamoto, T. Okuda, A. Kimura, H. Namatame, M. Taniguchi, and T. Aruga, *Phys. Rev. B* **82**, 201307(R) (2010).
- <sup>22</sup>M. Bedzyk and G. Materlik, *Surf. Sci.* **152/153**, 10 (1985).
- <sup>23</sup>R. G. Jones, *Prog. Surf. Sci.* **27**, 25 (1988).
- <sup>24</sup>M. Fouchier, M. T. McEllistrem, and J. J. Boland, *Surf. Sci.* **385**, L905 (1997).
- <sup>25</sup>N. D. Spencer, P. J. Goddard, P. W. Davies, M. Kitson, and R. M. Lambert, *J. Vac. Sci. Technol. A* **1**, 1554 (1983).
- <sup>26</sup>A. Barbieri and M. A. Van Hove, Symmetrized Automated Tensor Leed (SATLEED) package available from M. A. Van Hove, <http://www.ap.cityu.edu.hk/personal-website/Van-Hove.htm>.
- <sup>27</sup>J. B. Pendry, *J. Phys. C* **13**, 937 (1980).
- <sup>28</sup>T. Okuda, Y. Takeichi, Y. Maeda, A. Harasawa, I. Matsuda, T. Kinoshita, and A. Kakizaki, *Rev. Sci. Instrum.* **79**, 123117 (2008).
- <sup>29</sup>P. Blaha, K. Schwarz, G. K. H. Madsen, K. Kvasnicka, and J. Luitz, *An Augmented Plane Wave + Local Orbitals Program for Calculating Crystal Properties* (Karlheinz Schwarz, Techn. Universität Wien, Wien, Austria, 2001).
- <sup>30</sup>J. P. Perdew, K. Burke, and M. Ernzerhof, *Phys. Rev. Lett.* **77**, 3865 (1996).
- <sup>31</sup>W. A. Harrison, *Electronic Structure and the Properties of Solids: The Physics of the Chemical Bond* (Freeman, San Francisco, 1980).
- <sup>32</sup>D. J. Chadi, *Phys. Rev. B* **16**, 790 (1977).
- <sup>33</sup>E. Tamura, W. Piepke, and R. Feder, *Phys. Rev. Lett.* **59**, 934 (1987).
- <sup>34</sup>J. Henk, T. Scheunemann, S. V. Halilov, and R. Feder, *J. Phys.: Condens. Matter* **8**, 47 (1996).
- <sup>35</sup>J. H. Dil, *J. Phys.: Condens. Matter* **21**, 403001 (2009).
- <sup>36</sup>A. D. Becke and E. R. Johnson, *J. Chem. Phys.* **124**, 221101 (2006).
- <sup>37</sup>F. Tran and P. Blaha, *Phys. Rev. Lett.* **102**, 226401 (2009).
- <sup>38</sup>C. D. Thurmond, *J. Electrochem. Soc.* **122**, 1133 (1975).
- <sup>39</sup>A. Kimura, E. E. Krasovskii, R. Nishimura, K. Miyamoto, T. Kadono, K. Kanomaru, E. V. Chulkov, G. Bihlmayer, K. Shimada, H. Namatame, and M. Taniguchi, *Phys. Rev. Lett.* **105**, 076804 (2010).
- <sup>40</sup>S.-J. Tang, T.-R. Chang, C.-C. Huang, C.-Y. Lee, C.-M. Cheng, K.-D. Tsuei, H.-T. Jeng, and C.-Y. Mou, *Phys. Rev. B* **81**, 245406 (2010).
- <sup>41</sup>S. Kotochigova, Z. H. Levine, E. L. Shirley, M. D. Stiles, and C. W. Clark, *Phys. Rev. A* **55**, 191 (1997); <http://physics.nist.gov/PhysRefData/DFTdata/>.